Steel and Composite Structures, *Vol. 29, No. 1 (2018) 53-66*
DOI: https://doi.org/10.12989/scs.2018.29.1.053

A high-order gradient model for wave propagation analysis of porous FG nanoplates

Davood Shahsavari [1], Behrouz Karami [*1] and Li Li [2]

[1] *Department of Mechanical Engineering, Marvdasht Branch, Islamic Azad University, Marvdasht, Iran*
[2] *State Key Laboratory of Digital Manufacturing Equipment and Technology, School of Mechanical Science and Engineering, Huazhong University of Science and Technology, Wuhan 430074, China*

(*Received April 25, 2018, Revised July 31, 2018, Accepted August 17, 2018*)

Abstract. A high-order nonlocal strain gradient model is developed for wave propagation analysis of porous FG nanoplates resting on a gradient hybrid foundation in thermal environment, for the first time. Material properties are assumed to be temperature-dependent and graded in the nanoplate thickness direction. To consider the thermal effects, uniform, linear, nonlinear, exponential, and sinusoidal temperature distributions are considered for temperature-dependent FG material properties. On the basis of the refined-higher order shear deformation plate theory (R-HSDT) in conjunction with the bi-Helmholtz nonlocal strain gradient theory (B-H NSGT), Hamilton's principle is used to derive the equations of wave motion. Then the dispersion relation between frequency and wave number is solved analytically. The influences of various parameters (such as temperature rise, volume fraction index, porosity volume fraction, lower and higher order nonlocal parameters, material characteristic parameter, foundations components, and wave number) on the wave propagation behaviors of porous FG nanoplates are investigated in detail.

Keywords: nanoporous materials; wave propagation; bi-Helmholtz nonlocal strain gradient theory; higher-order shear deformation plate theory; thermal loadings

1. Introduction

Functionally graded materials (FGMs) are viewed as a new class of composite materials, in which material properties continuously and smoothly change from the surface of one side to the surface of the other side. Unlike laminated composite materials, FGM removes the delamination, stress concentration, and matrix cracking phenomena. Recently, a new group of plates made of FGMs (involving metal and ceramic phases) has attracted much interest in engineering applications. Because the ceramic component supports high thermal resistance while the metal component gives a reliable mechanical performance in the composite structural system for reduction of the probability of fracture. As one of the pioneering studies on FG plates, the static and dynamic responses of the FG plates by varying the volume fraction of the metallic and ceramic components using a simple power-law distribution function were studied by (Praveen and Reddy 1998). (Huang and Shen 2004) examined the influence of thermal environment on the nonlinear frequency and dynamic displacement behavior of FG plates using a higher-order shear deformation plate theory in conjunction with perturbation technique. It was shown that the environmental temperature possesses considerable role on determining the behaviors of FG plates. Thermo-mechanical dynamics response of perfect and imperfect microbeams with temperature-dependent and size-dependent materials was investigated by (Farokhi and Ghayesh 2015).

It is known that in the process of FGM fabrication, micro-voids (so-called porosities) can occur inside the materials during the sintering process (Zhu *et al*. 2001, Li *et al*. 2003). This occurrence is relevant to the vast difference in solidification temperatures between material components (Zhu *et al*. 2001). In view of FG plates, a number of studies were focused on the porosity effect. For example, (Yahia *et al*. 2015) investigated the wave propagation in FG plates with porosities in the absence of thermal effect based on various higher-order shear deformation plate theories. (Gupta and Talha 2017) further investigated the influence of porosity on the free vibration behavior of FG plates in the presence of a thermal effect using a non-polynomial higher-order shear and normal deformation theory. More recently, (Shahsavari *et al*. 2018b) studied the vibrational behavior of FG plates with three different porosity patterns using a novel quasi-3D shear deformation theory.

In order to reduce the number of variables used in the equilibrium equations (in comparison of higher-order shear deformation theories (HSDTs)) and satisfy the shear deformation effects on the bottom and top surfaces of plate structures (in comparison of classical plate theory (CPT)), a refined theory with only two variables was presented by (Mechab *et al*. 2010) under the name of the refined-plate theory (RPT) for studying the mechanical behavior of isotropic plates. Furthermore, the RPT does not have any shear correction factor, as used in the first-order shear

*Corresponding author, Ph.D. Student,
E-mail: behrouz.karami@miau.ac.ir

ISSN: 1229-9367 (Print), 1598-6233 (Online)

deformation plate theory (FSDT).

Based on the RPT, different mechanical investigations were presented for micro/nano-scale isotropic (Shimpi and Patel 2006a, Klouche *et al*. 2017, Shahsavari and Janghorban 2017, Shahsavari *et al*. 2017, 2018a), FGMs (Zidi *et al*. 2017, Elmossouess *et al*. 2017, Hachemi *et al*. 2017, Sekkal *et al*. 2017, Bellifa *et al*. 2017, Meftah *et al*. 2017, Karami *et al*. 2018e), and laminated microplates (Thai and Kim 2012, Sehoul *et al*. 2017, Merdaci *et al*. 2016). Then, the various models of the RPT under the influence of different shape functions by dividing the transverse displacement into bending and shear parts for plate structures were developed.

Despite the wide capacity of classical continuum theories (e.g., CPT, FSDT, HSDT, and R-HSDTs) for determining the behaviors of plates, the characteristics of micro/-nanoplates cannot be predicted accurately using these theories since the interactions between atoms are not ignorable. That is, we should take into account the size-dependent effects on the mechanical behavior of structures at small scales. Recently, size-dependent continuum theories are proposed by introducing various length-scale parameters in their constitutive relations. Up to now, a great deal of attention has been devoting to the size effects of mechanical characteristics of microscale structures (such as beams, plates, and shells) (Ghayesh *et al*. 2013a, b, c, d, 2014, 2017, Gholipour *et al*. 2015, Farokhi *et al*. 2013, Ghayesh 2018a, b, c, d, Shimpi and Patel 2006b, Narendar and Gopalakrishnan 2012, Karami *et al*. 2018d). Recently, the size-dependent oscillations of functionally graded microbeams were investigated using the modified couple stress theory along with the Mori–Tanaka homogenisation technique by Ghayesh *et al*. (2017). However, there are few models concerning these structures whose scales tend to nanosize. Among non-classical continuum theories, the nonlocal elasticity theory (NET) has been proposed by (Eringen 1983) to consider the size-dependent effects by defining that the stress at a point of the domain is dependent on the stress in neighboring points in that domain. It is worth emphasizing that in this theory, the influence of long-range inter-atomic forces is described explicitly by only one small-scale parameter (so-called the nonlocal parameter). As a popular model, the NET has been largely used for the modeling of different nanostructures because of its simplicity (Karami *et al*. 2018a, j). However, with the increasing expansion of nanotechnology, the need for precise mechanical measurement at the nanoscale is becoming to an important challenge. So, the applicability of bi-Helmholtz nonlocal elasticity theory (B-H NET) (Lazar *et al*. 2006) including two distinct nonlocal parameters (lower and higher order nonlocal parameters) was examined by Koutsoumaris *et al*. (2015). It was shown that the B-H NET can produce a larger softening-stiffness effect than NET with increasing the nonlocal parameters. Hence, B-H NET model is more suitable than one parameter nonlocal model (NET) in dealing with softening predicaments in nanoscaled structures (see, e.g., carbon nanotubes). However, the capability of the nonlocal models (NET and B-H NET) for predicting other size-dependent mechanisms may exist some limited problems (Lim *et al*. 2015). For example, by applying a nonlocal model, the stiffness-enhancement mechanism that has been seen via the strain gradient elasticity theory (SGT) (Lam *et al*. 2003) and as well as experimental researches (Lin *et al*. 2013) cannot be predicted well. To fix this drawback, (Askes and Aifantis 2009) proposed a nonlocal strain gradient theory (NSGT) for the analysis of the size-dependent wave propagation behavior of carbon nanotubes. When rewritten Hooke's law corresponding to the NSGT, the nonlocal parameter as the representative of NET is used on the Laplacian of stress on the left side of the constitutive equations to capture the softening-stiffness mechanism and the material characteristic parameter as the representative of SGT is considered on the right side of the equations on the Laplacian of strains to capture the stiffness-enhancement mechanism. Accordingly, the size-dependent effects such like softening-stiffness and stiffness-enhancement are estimated with two small-scale parameters using NSGT. Next (Lim *et al*. 2015) proposed a higher-order NSGT relying on the thermodynamics framework. The matching between ready results with this theory in comparison with experimental data and molecular simulation (MD) results has been more than both of the NET and SGT (Lim *et al*. 2015). Later, the NSGT has been widely used for capturing the size-dependencies response of nanostructures systems (Karami *et al*. 2018b, c, f, g, h, i, 2017, Barati 2017b, Ebrahimi and Dabbagh 2018, She *et al*. 2017, 2018). The works are studied based on the NSGT of Helmholtz type. In the case of the NSGT bi-Helmholtz type, it is more likely to have a better match with experimental data due to its high-order terms. More recently, on the basis of the NSGT bi-Helmholtz type, Barati and Zenkour examined the wave behavior of porous double-nanobeam systems for nanobeam structures without (Barati and Zenkour 2017) and with considering of the uniform thermal loads (Barati 2017a).

With respond to open literature, up to now, no study has been carried out to use a model of bi-Helmholtz nonlocal strain gradient elasticity theory (B-H NSGT) for research on plates. Also, in view of all that has been reviewed so far, very few studies have tried to provide the analytical solution for analysis of FG nanoplates including porosities embedded in a gradient hybrid foundation. To eliminate mentioned limitations, in this study, we consider porous FG nanoplates embedded within gradient hybrid foundation substrate and thermal environment. The presented paper will be focused on the size-dependent wave propagation analysis. The size-dependent effects are taken into account by employing a high-order nonlocal strain gradient theory (or bi-Helmholtz nonlocal elasticity theory (B-H NET)) containing three small-scale parameters for more accurate analysis. Furthermore, to consider the thermal effects on the wave behavior of graded nanoplates, uniform, linear, nonlinear, exponential, and sinusoidal temperature distributions are considered for temperature-dependent FG material properties. The displacement form of the governing equations will be derived based on a refined higher-order shear deformation plate theory in conjunction with the B-H NSGT, and will be solved by using an analytical method. Finally, different parameter effects (such as temperature rise, volume fraction index, porosity volume fraction, lower

and higher order nonlocal parameters, material characteristic parameter, foundations components, and wave number) on the wave characteristics of porous nanoplates will be investigated in detail.

2. Preliminary concepts and definitions

Consider a rectangular nanoplate made of FGMs, referred to the Cartesian coordinate (x, y, z), shown in Fig. 1. Let the length of the nanoplate along the x-direction, the width along the y-direction and the thickness along z-direction be a, b and h, respectively. Furthermore, we consider a nanoplate resting on a gradient hybrid foundation.

2.1 Porosity-dependent functionally graded materials

The material composition is assumed to be varied along the thickness direction of nanoplate as follow (Li and Hu 2016a)

$$P\left(z\right)=P_{\mathrm{m}}V_{\mathrm{m}}+P_{\mathrm{c}}V_{\mathrm{c}} \tag{1}$$

in which P_m and P_c are, respectively, the effective material properties of the metal and ceramic phases; V_m and V_c are the volume fraction of the metal and ceramic phases, respectively. Note that the through-thickness distribution of a material property $P(z)$ (i.e., Young's modulus E, Poisson's ratio v, shear modulus G, and mass density ρ) can be defined by using the modified rule of mixture (Eq. (1)). It has been shown that, for an Al/SiC FG material, composite, the modified rule of the mixture can be applied for accurately predicting Young's modulus (Bhattacharyya *et al*. 2007).

On the basis of the power-law distribution function for FGM (P-FGM model), we obtain the distribution of volume fraction of the ceramic and metal phases (Wattanasakulpong and Ungbhakorn 2014)

$$\begin{aligned} V_{\mathrm{c}}&=\left(\frac{1}{2}+\frac{z}{h}\right)^{p}-\frac{\xi}{2}\\ V_{\mathrm{m}}&=1-\left(\frac{1}{2}+\frac{z}{h}\right)^{p}-\frac{\xi}{2}\end{aligned} \tag{2}$$

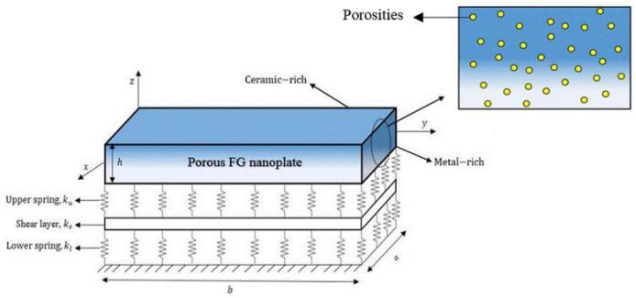

Fig. 1 The configuration of an imperfect FG nanoplate with porosities resting on gradient hybrid foundation

in which z is the direction from the mid-plane of the FG plate. Here the FG power index p is related to the change of volume fraction in the material composition, and ξ is the volume fraction of porosity. Noting that, without porosity, the power-law distribution function was found to be consistent for different volume fractions of two-phase FG material by using experiment data (Kapuria *et al*. 2008).

Based on the assumptions mentioned above, the material properties of the porous FG plates are obtained as

$$P\left(z\right)=P_{\mathrm{m}}+\left(P_{\mathrm{c}}-P_{\mathrm{m}}\right)\left(\frac{1}{2}+\frac{z}{h}\right)^{p}-\frac{\xi}{2}\left(P_{\mathrm{c}}+P_{\mathrm{m}}\right) \tag{3}$$

In the case of p = 0, the material of the plate is pure ceramic, and a pure metal is recovered when $p \to +\infty$. Moreover, the increment of p increases the metal volume fraction (Azadi *et al*. 2014). Thus, Young's modulus E, Poisson's ratio v, thermal distribution α, thermal conductivity κ, shear modulus G, and mass density ρ of the nanoscale plate can be expressed by Eq. (3).

2.2 Temperature-dependent material properties

In the case of nonlinear thermo-elasticity, temperature-dependent material property P (metal or ceramic phase) can be written as (Touloukian and Ho 1970)

$$\mathrm{P}=\mathrm{P}_{0}\left(\mathrm{P}_{-1}T^{-1}+\mathrm{P}_{1}T+\mathrm{P}_{2}T^{2}+\mathrm{P}_{3}T^{3}+1\right) \tag{4}$$

Here P_0, P_{-1}, P_1, P_2 and P_3 are the temperature-dependent coefficients, which are need to be uniquely determined for a specified material (see Ref. Reddy and Chin 1998). In the case of most materials, P_{-1} = 0. Thus, the previous equation can be reduced to $P = P_0(1 + P_1T + P_2T^2 + P_3T^3)$.

Generally, three cases of temperature rise across the thickness are presented for FG plates (i.e. uniform, linear and nonlinear temperature rises). Also, two interested cases (exponential and sinusoidal models) have been added for presenting a comprehensive study in FG plates accounting for the influence of thermal change.

2.2.1 Uniform temperature rise

The uniform case temperature rise can be defined by (Li *et al*. 2009)

$$T\left(z\right)=T_{0}+\Delta T\left(z\right) \tag{5}$$

Often the initial temperature T_0 is the temperature of the surface with pure metal T_m and equals the room temperature (i.e., $T_0 = T_m$ = 300 K), and $\Delta T(z) = T_c - T_m$ where T_c denotes the temperature of the surface with pure ceramic.

2.2.2 Linear temperature rise

According to the assumptions of the previous section, the temperature distribution along the thickness direction can be expressed as the following form with linear temperature rise from T_c to T_m (Li *et al*. 2009).

$$T\left(z\right)=\frac{\left(T_{\mathrm{c}}+T_{\mathrm{m}}\right)}{2}-\left(T_{\mathrm{c}}-T_{\mathrm{m}}\right)\frac{z}{h} \tag{6}$$

2.2.3 Nonlinear temperature rise

This section is based on the assumption that temperature distribution is only in the thickness direction and the temperature field in the *x-y* plane of the plate is assumed to be constant. In this non-linear case, one-dimensional steady-state heat conduction equation is applied for the temperature field in the thickness direction and can be given by (Li *et al*. 2009)

$$-\frac{d}{dz}\left(\kappa(z)\frac{dT}{dz}\right)=0 \tag{7}$$

On the basis of power-law distribution and under the temperature boundary conditions $T = T_c$ at $z=\frac{h}{2}$, and $T = T_m$ at $z=-\frac{h}{2}$, the solution of Eq. (7) can be expressed as a series of polynomials

$$T(z)=T_{\mathrm{m}}+(T_{\mathrm{c}}-T_{\mathrm{m}})\eta(z) \tag{8}$$

in which

$$\begin{aligned}\eta(z)=\frac{1}{C}\Bigg[&\left(\frac{2z+h}{2h}\right)-\frac{\kappa_{\mathrm{cm}}}{(N+1)\kappa_{\mathrm{m}}}\left(\frac{2z+h}{2h}\right)^{N+1}\\&+\frac{\kappa_{\mathrm{cm}}^2}{(2N+1)\kappa_{\mathrm{m}}^2}\left(\frac{2z+h}{2h}\right)^{2N+1}-\frac{\kappa_{\mathrm{cm}}^3}{(3N+1)\kappa_{\mathrm{m}}^3}\left(\frac{2z+h}{2h}\right)^{3N+1}\\&+\frac{\kappa_{\mathrm{cm}}^4}{(4N+1)\kappa_{\mathrm{m}}^2}\left(\frac{2z+h}{2h}\right)^{4N+1}-\frac{\kappa_{\mathrm{cm}}^5}{(5N+1)\kappa_{\mathrm{m}}^2}\left(\frac{2z+h}{2h}\right)^{5N+1}\Bigg]\end{aligned} \tag{9}$$

$$\begin{aligned}C=1&-\frac{\kappa_{\mathrm{cm}}}{(N+1)\kappa_{\mathrm{m}}}+\frac{\kappa_{\mathrm{cm}}^2}{(2N+1)\kappa_{\mathrm{m}}^2}-\frac{\kappa_{\mathrm{cm}}^3}{(3N+1)\kappa_{\mathrm{m}}^3}\\&+\frac{\kappa_{\mathrm{cm}}^4}{(4N+1)\kappa_{\mathrm{m}}^4}-\frac{\kappa_{\mathrm{cm}}^5}{(5N+1)\kappa_{\mathrm{m}}^5}\end{aligned} \tag{10}$$

Here $\kappa_{cm} = \kappa_c - \kappa_m$ in which κ_c and κ_m are thermal conductivity of the bottom and top surfaces, respectively.

2.2.4 Exponential temperature rise

The exponentially temperature rise along the thickness direction can be expressed as (Gupta and Talha 2017)

$$T(z)=T_{\mathrm{c}}\left[e^{-(1/2)\log(T_{\mathrm{c}}/T_{\mathrm{m}})(1-(2z/h))}\right] \tag{11}$$

with $T\left(\frac{h}{2}\right)=T_c,\ T\left(-\frac{h}{2}\right)=T_m.$

2.2.5 Sinusoidal temperature rise

In the case of sinusoidal temperature rise, the temperature rise can be defined as follow (Gupta and Talha 2017)

$$T(z)=\frac{(T_{\mathrm{c}}+T_{\mathrm{m}})}{2}-\frac{(T_{\mathrm{c}}-T_{\mathrm{m}})}{2}\cos\left(\frac{\pi}{2}+\frac{\pi z}{h}\right) \tag{12}$$

with $T\left(\frac{h}{2}\right)=T_c,\ T\left(-\frac{h}{2}\right)=T_m.$

3. Size-dependent equations of wave motion

For consideration of the small-scale effects on the nanostructure systems, size-dependent equations of wave motion will be derived on the basis of the bi-Helmholtz nonlocal strain gradient elasticity theory. For the purposes of taking into account the shear deformation, it is necessary to consider the higher-order shear deformation plate theory.

3.1 Kinematic relation

The refined-higher-order shear deformation plate theory (R-HSDT) adopted in the present work which yields the following displacement field (Shimpi 2002)

$$\begin{aligned}u(x,y,z,t)&=u_0(x,y,t)-z\frac{\partial w_b}{\partial x}-f(z)\frac{\partial w_s}{\partial x}\\v(x,y,z,t)&=v_0(x,y,t)-z\frac{\partial w_b}{\partial y}-f(z)\frac{\partial w_s}{\partial y}\\w(x,y,t)&=w_b(x,y,t)+w_s(x,y,t)\end{aligned} \tag{13}$$

where u_0 and v_0 are respectively the displacements on the middle surface along x and y directions; w_b, w_s are respectively the bending and shear displacements. $f(z)$ is the shape function which denotes the distribution of transverse shear stress or strain along the thickness direction. In this study, we assume algebraical shape function as $f(z) = g(z) + \aleph(z)$ (Sarangan and Singh 2016)
where

$$g(z)=h\left(\frac{m^2z^2}{h^2}+1\right)\ \text{ and }\ \aleph(z)=-\frac{8mh^2}{\left(m^3h^3+8h^3\right)},$$

in which $m = 2$.

By using the well-known geometric relations, non-zero strain–displacement relations can be written as

$$\begin{aligned}&\begin{Bmatrix}\varepsilon_{xx}\\ \varepsilon_{yy}\\ \gamma_{xy}\end{Bmatrix}=\begin{Bmatrix}\varepsilon_{xx}^0\\ \varepsilon_{yy}^0\\ \gamma_{xy}^0\end{Bmatrix}+z\begin{Bmatrix}K_{xx}\\ K_{yy}\\ K_{xy}\end{Bmatrix}+f(z)\begin{Bmatrix}K'_{xx}\\ K'_{yy}\\ K'_{xy}\end{Bmatrix}\\&,\begin{Bmatrix}\gamma_{yz}\\ \gamma_{xz}\end{Bmatrix}=g(z)\begin{Bmatrix}\gamma_{yz}^0\\ \gamma_{xz}^0\end{Bmatrix}\end{aligned} \tag{14}$$

here (ε_x, ε_y) are the normal strains, and (γ_{xy}, γ_{yz}, γ_{xz}) are the shear strains. They can be defined by

$$\begin{aligned}&\begin{bmatrix}\varepsilon_{xx}^0\\ \varepsilon_{yy}^0\\ \varepsilon_{xy}^0\end{bmatrix}=\begin{Bmatrix}\frac{\partial u_0}{\partial x}\\ \frac{\partial v_0}{\partial y}\\ \frac{\partial u_0}{\partial y}+\frac{\partial v_0}{\partial x}\end{Bmatrix},\begin{bmatrix}K_{xx}\\ K_{yy}\\ K_{xy}\end{bmatrix}=\begin{Bmatrix}-\frac{\partial^2 w_b}{\partial x^2}\\ -\frac{\partial^2 w_b}{\partial y^2}\\ -2\frac{\partial^2 w_b}{\partial x\,\partial y}\end{Bmatrix}\\&,\begin{bmatrix}K'_{xx}\\ K'_{yy}\\ K'_{xy}\end{bmatrix}=\begin{Bmatrix}-\frac{\partial^2 w_s}{\partial x^2}\\ -\frac{\partial^2 w_s}{\partial y^2}\\ -2\frac{\partial^2 w_s}{\partial x\,\partial y}\end{Bmatrix},\begin{bmatrix}\gamma_{yz}^0\\ \gamma_{xz}^0\end{bmatrix}=\begin{Bmatrix}\frac{\partial w_s}{\partial y}\\ \frac{\partial w_s}{\partial x}\end{Bmatrix}\end{aligned} \tag{15}$$

and

$$g(z)=1-\frac{df(z)}{dz} \tag{16}$$

Within the framework of linear thermoelasticity, the Euler–Lagrange equations of FG nanoplate in the thermal environment are described as the following form based on Hamilton's principles.

$$\int_0^t \delta(U-K+W)dt=0 \tag{17}$$

in which δU, δK and δW are the variations of strain energy, kinetic energy and work done by external (applied) forces, respectively. The variation of strain energy is defined by

$$\delta U=\int \sigma_{ij}\delta\varepsilon_{ij}dV=\begin{bmatrix}\sigma_x\delta\varepsilon_x+\sigma_y\delta\varepsilon_y+\tau_{xy}\delta\gamma_{xy}\\+\tau_{yz}\delta\gamma_{yz}+\tau_{xz}\delta\gamma_{xz}\end{bmatrix}dV \tag{18}$$

Substituting Eqs. (14) and (15) into Eq. (18) yields

$$\delta U=\int_0^L\begin{bmatrix}N_x\dfrac{\partial\delta u_0}{\partial x}-M_x^b\dfrac{\partial^2\delta w_b}{\partial x^2}-M_x^s\dfrac{\partial^2\delta w_s}{\partial x^2}\\+N_y\dfrac{\partial\delta v_0}{\partial x}-M_y^b\dfrac{\partial^2\delta w_b}{y}-M_y^s\dfrac{\partial^2\delta w_s}{\partial y^2}\\+N_{xy}\left(\dfrac{\partial\delta u_0}{\partial y}+\dfrac{\partial\delta v_0}{\partial x}\right)-2M_{xy}^b\dfrac{\partial^2\delta w_b}{\partial x\,\partial y}\\-2M_{xy}^s\dfrac{\partial^2\delta w_s}{\partial x\,\partial y}+Q_{yz}\dfrac{\partial\delta w_s}{\partial y}+Q_{xz}\dfrac{\partial\delta w_s}{\partial x}\end{bmatrix}dx \tag{19}$$

where the stress resultants are defined as

$$\left\{N_i,M_i^b,M_i^s\right\}=\int\left\{1,z,f(z)\right\}\sigma_i dA,\ i=(x,y,xy) \tag{20}$$

$$Q_i=\int g(z)\sigma_i dA,\ i=(xz,yz) \tag{21}$$

The variation of external work caused by the applied forces on the FG nanoplates can be defined by the following equation

$$\delta W=\int_0^L\begin{bmatrix}N_x^0\dfrac{\partial(w_b+w_s)}{\partial x}\dfrac{\partial\delta(w_b+w_s)}{\partial x}\\+N_y^0\dfrac{\partial(w_b+w_s)}{\partial y}\dfrac{\partial\delta(w_b+w_s)}{\partial y}\\+2\delta N_{xy}^0\dfrac{\partial(w_b+w_s)}{\partial x}\dfrac{\partial(w_b+w_s)}{\partial y}\\+\left(q_{\text{Hybrid foundation}}\right)\delta(w_b+w_s)\end{bmatrix}dx \tag{22}$$

in which $N_x^0=N_y^0=N^T$ and $N_{xy}^0=0$ and

$$N^T=\int_{-\frac{h}{2}}^{\frac{h}{2}}\frac{E(z)}{1-\nu(z)}\alpha(z,T)T(z)dz \tag{23}$$

The distributed reaction between gradient hybrid foundation and the low surface of FG nanoplate can be expressed by Rad (2015)

$$\begin{aligned}&q_{\text{Hybrid foundation}}-\left(\frac{k_s}{k_l+k_u}\right)\nabla^2 q_{\text{Hybrid foundation}}\\&=\left(\frac{k_l k_u}{k_l+k_u}\right)(w_b+w_s)-\left(\frac{k_s k_u}{k_l+k_u}\right)\nabla^2(w_b+w_s)\end{aligned} \tag{24}$$

The variation of Kinetic energy based on the R-HSDT can be obtained as

$$\delta K=\int\left\{\left[\dot u_0\delta\dot u_0+\dot v_0\delta\dot v_0+\dot w\,\delta\dot w\right]\rho(z)\right\}dV$$
$$=\int_0^L\left\{\begin{bmatrix}I_0\left[\dot u_0\delta\dot u_0+\dot v_0\delta\dot v_0+(\dot w_b+\dot w_s)(\delta\dot w_b+\delta\dot w_s)\right]\\-I_1\left[\dot u_0\dfrac{\partial\delta\dot w_b}{\partial x}+\dfrac{\partial\dot w_b}{\partial x}\delta\dot u_0+\dot v_0\dfrac{\partial\delta\dot w_s}{\partial y}+\dfrac{\partial\dot w_s}{\partial y}\delta\dot v_0\right]\\-J_1\left[\dot u_0\dfrac{\partial\delta\dot w_s}{\partial x}+\dfrac{\partial\dot w_s}{\partial x}\delta\dot u_0+\dot v_0\dfrac{\partial\delta\dot w_s}{\partial y}+\dfrac{\partial\dot w_s}{\partial y}\delta\dot v_0\right]\\+I_2\left[\dfrac{\partial\delta\dot w_b}{\partial x}\dfrac{\partial\dot w_b}{\partial x}+\dfrac{\partial\delta\dot w_b}{\partial y}\dfrac{\partial\dot w_b}{\partial y}\right]\\+K_2\left[\dfrac{\partial\delta\dot w_s}{\partial x}\dfrac{\partial\dot w_s}{\partial x}+\dfrac{\partial\delta\dot w_s}{\partial y}\dfrac{\partial\dot w_s}{\partial y}\right]\\+J_2\left[\dfrac{\partial\dot w_b}{\partial x}\dfrac{\partial\delta\dot w_s}{\partial x}+\dfrac{\partial\dot w_s}{\partial x}\dfrac{\partial\delta\dot w_b}{\partial x}+\dfrac{\partial\dot w_b}{\partial y}\dfrac{\partial\delta\dot w_s}{\partial y}+\dfrac{\partial\dot w_s}{\partial y}\dfrac{\partial\delta\dot w_b}{\partial y}\right]\end{bmatrix}dA\right\}dx \tag{25}$$

in which the mass moments of inertias defined by

$$\begin{aligned}&\left\{I_0,I_1,I_2,J_1,J_2,K_2\right\}\\&=\int_{-\frac{h}{2}}^{\frac{h}{2}}\left\{1,z,z^2,f(z),zf(z),f^2(z)\right\}\rho(z)dz\end{aligned} \tag{26}$$

Noting that, in Eq. (25), the dot-superscript represents the differentiation with respect to time. Equilibrium equations in conjunction with Euler–Lagrange equations for a FG plate consists of metal and ceramic materials can be obtained as the following forms by substituting the expressions for δU, δK and δT from Eqs. (15), (22), and (25) into Eq. (17). Euler–Lagrange equations corresponding to the coefficients of δu_0, δv_0 and δw_b and δw_s are listed as below

$$\frac{\partial N_x}{\partial x}+\frac{\partial N_{xy}}{\partial y}=I_0\ddot u_0-I_1\frac{\partial\ddot w_b}{\partial x}-J_1\frac{\partial\ddot w_s}{\partial x} \tag{27}$$

$$\frac{\partial N_{xy}}{\partial x}+\frac{\partial N_y}{\partial y}=I_0\ddot v_0-I_1\frac{\partial\ddot w_b}{\partial y}-J_1\frac{\partial\ddot w_s}{\partial y} \tag{28}$$

$$\frac{\partial^2 M_x^b}{\partial x^2}+2\frac{\partial^2 M_{xy}^b}{\partial x\,\partial y}+\frac{\partial^2 M_y^b}{\partial y^2}-\left(\frac{k_l k_u}{k_l+k_u}\right)\left(w_b+w_s\right)$$
$$-\left\{N^T-\left(\frac{k_s k_u}{k_l+k_u}\right)\right\}\nabla^2\left(w_b+w_s\right) \quad (29)$$
$$=I_0\left(\ddot{w}_b+\ddot{w}_s\right)+I_1\left(\frac{\partial\ddot{u}_0}{\partial x}+\frac{\partial\ddot{v}_0}{\partial y}\right)-I_2\nabla^2\ddot{w}_b-J_2\nabla^2\ddot{w}_s$$

$$\frac{\partial^2 M_x^s}{\partial x^2}+2\frac{\partial^2 M_{xy}^s}{\partial x\,\partial y}+\frac{\partial^2 M_y^s}{\partial y^2}+\frac{\partial Q_{xz}}{\partial x}+\frac{\partial Q_{yz}}{\partial y}$$
$$-\left\{N^T-\left(\frac{k_s k_u}{k_l+k_u}\right)\right\}\nabla^2\left(w_b+w_s\right)-\left(\frac{k_l k_u}{k_l+k_u}\right)\left(w_b+w_s\right) \quad (30)$$
$$=I_0\left(\ddot{w}_b+\ddot{w}_s\right)+J_1\left(\frac{\partial\ddot{u}_0}{\partial x}+\frac{\partial\ddot{v}_0}{\partial y}\right)-J_2\nabla^2\ddot{w}_b-K_2\nabla^2\ddot{w}_s$$

3.2 Bi-Helmholtz nonlocal strain gradient elasticity theory

The nonlocal strain gradient theory can be applied for investigating the size-dependent effects of both the long-range force and microstructural deformation mechanism. According to the nonlocal strain gradient theory, the total stress can be expressed as (Lim *et al*. 2015)

$$\sigma_{ij}=\sigma_{ij}^{(0)}-\nabla\sigma_{ij}^{(1)} \quad (31)$$

where the classical stress $\sigma_{ij}^{(0)}$ and the higher-order stress $\sigma_{ij}^{(1)}$ are related to the work conjugate of strain (ε_{ij}) and the work conjugate of strain gradient ($\nabla\varepsilon_{ij}$), respectively. They can be described as convolution integrals in a reference domain V over some nonlocal kernel functions

$$\sigma_{ij}^{(0)}=\int_0^L C_{ijkl}\,\alpha_0\left(x,x',e_0a\right)\varepsilon_{kl}'\left(x'\right)dx'$$
$$\sigma_{ij}^{(1)}=l^2\int_0^L C_{ijkl}\,\alpha_1\left(x,x',e_1a\right)\nabla\varepsilon_{kl}'\left(x'\right)dx' \quad (32)$$

Here α (x, x', e_0a) and α_1 (x, x', e_1a) are the nonlocal kernel functions that given by Eringen (1983). l represents a material characteristic parameter (in some available literature known as the length-scale parameter or gradient parameter (Karami and Janghorban, 2016, Nami and Janghorban, 2014)). e_0a and e_1a denote the lower and higher order nonlocal parameters. Here a is an internal characteristic length (e.g., lattice constant), and the material constants e_0 and e_1 are often determined experimentally or approximated by matching the dispersion relation of atomic lattice dynamics (Li and Hu 2016b, Li *et al*. 2016, Zhu and Li 2017). For the two-dimension (2D) problem, the linear nonlocal differential operator, which is written as the following form, is applied to the both sides of Eq. (31).

$$L_i=1-\left(e_i a\right)^2\nabla^2 \qquad \text{for} \qquad i=0,\,1 \quad (33)$$

where, $\nabla^2=\partial^2/\partial x^2+\partial^2/\partial y^2$ is the Laplacian operator for 2D problems in Cartesian coordinate.

Next, by applying Eq. (32) into Eq. (31), a general constitutive model for the size-dependent FG nanoplate can be defined as

$$\left[1-\left(e_1a\right)^2\nabla^2\right]\left[1-\left(e_0a\right)^2\nabla^2\right]\sigma_{ij}=C_{ijkl}\left[1-\left(e_1a\right)^2\nabla^2\right]\varepsilon_{kl}$$
$$-C_{ijkl}\,l^2\left[1-\left(e_0a\right)^2\nabla^2\right]\nabla^2\varepsilon_{kl} \quad (34)$$

or

$$\left(1-\mu_0^2\nabla^2\right)\left(1-\mu_1^2\nabla^2\right)\sigma_{ij}=C_{ijkl}\left(1-\mu_1^2\nabla^2\right)\varepsilon_{kl}$$
$$-C_{ijkl}\,l^2\left(1-\mu_0^2\nabla^2\right)\nabla^2\varepsilon_{kl} \quad (35)$$

Here for the sack of simplicity, we assume that μ_0 = (e_0a) and μ_1 = (e_1a). The previous equation is the constitutive equation of the bi-Helmholtz nonlocal strain gradient theory (B-H NSGT).

By using the strains of R-HSDT, we have

$$\left(1-\mu_0^2\nabla^2\right)\left(1-\mu_1^2\nabla^2\right)\begin{bmatrix}\sigma_{xx}\\ \sigma_{yy}\\ \sigma_{xy}\\ \sigma_{yz}\\ \sigma_{xz}\end{bmatrix}=\left(1-\mu_1^2\nabla^2-l^2\left(1-\mu_0^2\nabla^2\right)\nabla^2\right)$$
$$\begin{bmatrix}Q_{11}&Q_{12}&0&0&0\\ Q_{12}&Q_{22}&0&0&0\\ 0&0&Q_{66}&0&0\\ 0&0&0&Q_{44}&0\\ 0&0&0&0&Q_{55}\end{bmatrix}\begin{bmatrix}\varepsilon_x\\ \varepsilon_y\\ \gamma_{xy}\\ \gamma_{yz}\\ \gamma_{xz}\end{bmatrix} \quad (36)$$

in which Q_{ij} are defined as follows

$$Q_{11}=Q_{22}=\frac{E(z)}{\left(1-\nu^2\right)}$$
$$Q_{12}=\frac{E(z)\nu}{\left(1-\nu^2\right)} \quad (37)$$
$$Q_{44}=Q_{55}=Q_{66}=\frac{E(z)}{\left(2\left(1+\nu\right)\right)}$$

3.3 Governing equation

To calculate the force-strain and moment-strain of the imperfect (with porosity) FG plates, we get the following relations by the integration of Eq. (36) across the cross-section area of the plate.

$$\left(1-\mu_0^2\nabla^2\right)\left(1-\mu_1^2\nabla^2\right)\begin{bmatrix}N_x\\ N_y\\ N_{xy}\end{bmatrix}=\left(1-\mu_1^2\nabla^2-l^2\left(1-\mu_0^2\nabla^2\right)\nabla^2\right)$$
$$\left[\begin{pmatrix}A_{11}&A_{12}&0\\ A_{12}&A_{22}&0\\ 0&0&A_{66}\end{pmatrix}\begin{Bmatrix}\frac{\partial u_0}{\partial x}\\ \frac{\partial v_0}{\partial y}\\ \frac{\partial u_0}{\partial y}+\frac{\partial v_0}{\partial x}\end{Bmatrix}+\begin{pmatrix}B_{11}&B_{12}&0\\ B_{12}&B_{22}&0\\ 0&0&B_{66}\end{pmatrix}\begin{Bmatrix}-\frac{\partial^2 w_b}{\partial x^2}\\ -\frac{\partial^2 w_b}{\partial y^2}\\ -2\frac{\partial^2 w_b}{\partial x\,\partial y}\end{Bmatrix}\right. \quad (38)$$

$$+\begin{pmatrix} B_{11}^s & B_{12}^s & 0 \\ B_{12}^s & B_{22}^s & 0 \\ 0 & 0 & B_{66}^s \end{pmatrix}\left\{\begin{matrix} -\dfrac{\partial^2 w_s}{\partial x^2} \\ -\dfrac{\partial^2 w_s}{\partial y^2} \\ -2\dfrac{\partial^2 w_s}{\partial x\,\partial y} \end{matrix}\right\}\Bigg] \tag{38}$$

$$\left(1-\mu_0{}^2\nabla^2\right)\left(1-\mu_1{}^2\nabla^2\right)\begin{bmatrix} M_x^b \\ M_y^b \\ M_{xy}^b \end{bmatrix}=\left(1-\mu_1{}^2\nabla^2-l^2\left(1-\mu_0{}^2\nabla^2\right)\nabla^2\right)$$

$$\Bigg[\begin{pmatrix} B_{11} & B_{12} & 0 \\ B_{12} & B_{22} & 0 \\ 0 & 0 & B_{66} \end{pmatrix}\left\{\begin{matrix} \dfrac{\partial u_0}{\partial x} \\ \dfrac{\partial v_0}{\partial y} \\ \dfrac{\partial u_0}{\partial y}+\dfrac{\partial v_0}{\partial x} \end{matrix}\right\}+\begin{pmatrix} D_{11} & D_{12} & 0 \\ D_{12} & D_{22} & 0 \\ 0 & 0 & D_{66} \end{pmatrix}\left\{\begin{matrix} -\dfrac{\partial^2 w_b}{\partial x^2} \\ -\dfrac{\partial^2 w_b}{\partial y^2} \\ -2\dfrac{\partial^2 w_b}{\partial x\,\partial y} \end{matrix}\right\} \tag{39}$$

$$+\begin{pmatrix} D_{11}^s & D_{12}^s & 0 \\ D_{12}^s & D_{22}^s & 0 \\ 0 & 0 & D_{66}^s \end{pmatrix}\left\{\begin{matrix} -\dfrac{\partial^2 w_s}{\partial x^2} \\ -\dfrac{\partial^2 w_s}{\partial y^2} \\ -2\dfrac{\partial^2 w_s}{\partial x\,\partial y} \end{matrix}\right\}\Bigg]$$

$$\left(1-\mu_0{}^2\nabla^2\right)\left(1-\mu_1{}^2\nabla^2\right)\begin{bmatrix} M_x^s \\ M_y^s \\ M_{xy}^s \end{bmatrix}=\left(1-\mu_1{}^2\nabla^2-l^2\left(1-\mu_0{}^2\nabla^2\right)\nabla^2\right)$$

$$\Bigg[\begin{pmatrix} B_{11}^s & B_{12}^s & 0 \\ B_{12}^s & B_{22}^s & 0 \\ 0 & 0 & B_{66}^s \end{pmatrix}\left\{\begin{matrix} \dfrac{\partial u_0}{\partial x} \\ \dfrac{\partial v_0}{\partial y} \\ \dfrac{\partial u_0}{\partial y}+\dfrac{\partial v_0}{\partial x} \end{matrix}\right\}+\begin{pmatrix} D_{11}^s & D_{12}^s & 0 \\ D_{12}^s & D_{22}^s & 0 \\ 0 & 0 & D_{66}^s \end{pmatrix}\left\{\begin{matrix} -\dfrac{\partial^2 w_b}{\partial x^2} \\ -\dfrac{\partial^2 w_b}{\partial y^2} \\ -2\dfrac{\partial^2 w_b}{\partial x\,\partial y} \end{matrix}\right\} \tag{40}$$

$$+\begin{pmatrix} H_{11}^s & H_{12}^s & 0 \\ H_{12}^s & H_{22}^s & 0 \\ 0 & 0 & H_{66}^s \end{pmatrix}\left\{\begin{matrix} -\dfrac{\partial^2 w_s}{\partial x^2} \\ -\dfrac{\partial^2 w_s}{\partial y^2} \\ -2\dfrac{\partial^2 w_s}{\partial x\,\partial y} \end{matrix}\right\}\Bigg]$$

$$\left(1-\mu_0{}^2\nabla^2\right)\left(1-\mu_1{}^2\nabla^2\right)\begin{bmatrix} Q_{xz} \\ Q_{yz} \end{bmatrix}=$$

$$\left(1-\mu_1{}^2\nabla^2-l^2\left(1-\mu_0{}^2\nabla^2\right)\nabla^2\right)\begin{pmatrix} A_{44}^s & 0 \\ 0 & A_{55}^s \end{pmatrix}\left\{\begin{matrix} \dfrac{\partial w_s}{\partial x} \\ \dfrac{\partial w_s}{\partial y} \end{matrix}\right\} \tag{41}$$

in which the cross-sectional rigidities are obtained as

$$\begin{bmatrix} A_{11} & B_{11} & D_{11} & B_{11}^s & D_{11}^s & H_{11}^s \\ A_{12} & B_{12} & D_{12} & B_{12}^s & D_{12}^s & H_{12}^s \\ A_{66} & B_{66} & D_{66} & B_{66}^s & D_{66}^s & H_{66}^s \end{bmatrix} = \int_{-\frac{h}{2}}^{\frac{h}{2}} Q_{11}\left\{\begin{matrix} 1 \\ \nu \\ \dfrac{1-\nu}{2} \end{matrix}\right\}\left(1,z,z^2,f\ (z),zf\ (z),f^{\,2}(z)\right) \tag{42}$$

$$\left(A_{22},B_{22},D_{22},B_{22}^s,D_{22}^s,H_{22}^s\right)=\left(A_{11},B_{11},D_{11},B_{11}^s,D_{11}^s,H_{11}^s\right) \tag{43}$$

$$A_{44}^s=A_{55}^s=\int_{-\frac{h}{2}}^{\frac{h}{2}} Q_{44}\left[g\ (z)\right]^2 dz \tag{44}$$

By substituting Eqs. (38)-(41) into Eqs. (27)-(30), the governing equations for a FG nanoplate under the influence of thermal loading and gradient hybrid foundation can be expressed in terms of displacements (u_0, v_0, w_b, w_s) as follow

$$\begin{aligned}&\left(1-\mu_1{}^2\nabla^2-l^2\left(1-\mu_0{}^2\nabla^2\right)\nabla^2\right)\Bigg[A_{11}\frac{\partial^2 u_0}{\partial x^2}+\left(A_{12}+A_{66}\right)\frac{\partial^2 v_0}{\partial x\,\partial y}+A_{66}\frac{\partial^2 u_0}{\partial y^2}\\&-B_{11}\frac{\partial^3 w_b}{\partial x^3}-B_{11}^s\frac{\partial^3 w_s}{\partial x^3}-\left(B_{12}+2B_{66}\right)\frac{\partial^3 w_b}{\partial x\,\partial y^2}-\left(B_{12}^s+2B_{66}^s\right)\frac{\partial^3 w_s}{\partial x\,\partial y^2}\Bigg]\\&+\left(1-\mu_1{}^2\nabla^2\right)\left(1-\mu_0{}^2\nabla^2\right)\left[-I_0\ddot{u}_0+I_1\frac{\partial\ddot{w}_b}{\partial x}+J_1\frac{\partial\ddot{w}_s}{\partial x}\right]=0\end{aligned} \tag{45}$$

$$\begin{aligned}&\left(1-\mu_1{}^2\nabla^2-l^2\left(1-\mu_0{}^2\nabla^2\right)\nabla^2\right)\Bigg[A_{22}\frac{\partial^2 v_0}{\partial y^2}+\left(A_{12}+A_{66}\right)\frac{\partial^2 u_0}{\partial x\,\partial y}+A_{66}\frac{\partial^2 v_0}{\partial x^2}\\&-B_{22}\frac{\partial^3 w_b}{\partial y^3}-B_{22}^s\frac{\partial^3 w_s}{\partial y^3}-\left(B_{12}+2B_{66}\right)\frac{\partial^3 w_b}{\partial x^2\partial y}-\left(B_{12}^s+2B_{66}^s\right)\frac{\partial^3 w_s}{\partial x^2\partial y}\Bigg]\\&+\left(1-\mu_1{}^2\nabla^2\right)\left(1-\mu_0{}^2\nabla^2\right)\left[-I_0\ddot{v}_0+I_1\frac{\partial\ddot{w}_b}{\partial y}+J_1\frac{\partial\ddot{w}_s}{\partial y}\right]=0\end{aligned} \tag{46}$$

$$\begin{aligned}&\left(1-\mu_1{}^2\nabla^2-l^2\left(1-\mu_0{}^2\nabla^2\right)\nabla^2\right)\Bigg[B_{11}\frac{\partial^3 u_0}{\partial x^3}+\left(B_{12}+2B_{66}\right)\frac{\partial^3 u_0}{\partial x\,\partial y^2}\\&+B_{22}\frac{\partial^3 v_0}{\partial y^3}+\left(B_{12}+2B_{66}\right)\frac{\partial^3 v_0}{\partial x^2\partial y}-D_{11}\frac{\partial^4 w_b}{\partial x^4}-2\left(D_{12}+2D_{66}\right)\frac{\partial^4 w_b}{\partial x^2\partial y^2}\\&-D_{22}\frac{\partial^4 w_b}{\partial y^4}-D_{11}^s\frac{\partial^4 w_s}{\partial x^4}-2\left(D_{12}^s+2D_{66}^s\right)\frac{\partial^4 w_s}{\partial x^2\partial y^2}-D_{22}^s\frac{\partial^4 w_s}{\partial y^4}\Bigg]+\left(1-\mu_1{}^2\nabla^2\right)\\&\left(1-\mu_0{}^2\nabla^2\right)\Bigg[-I_0\left(\ddot{w}_b+\ddot{w}_s\right)-I_1\left(\frac{\partial\ddot{u}_0}{\partial x}+\frac{\partial\ddot{v}_0}{\partial y}\right)+I_2\nabla^2\left(\ddot{w}_b\right)+J_2\nabla^2\left(\ddot{w}_s\right)\\&-N^T\nabla^2\left(w_b+w_s\right)-\left(\frac{k_1k_u}{k_1+k_u}\right)\left(w_b+w_s\right)+\left(\frac{k_1k_u}{k_1+k_u}\right)\nabla^2\left(w_b+w_s\right)\Bigg]=0\end{aligned} \tag{47}$$

$$\left(1-\mu_1{}^2\nabla^2-l^2\left(1-\mu_0{}^2\nabla^2\right)\nabla^2\right)\Bigg[B_{11}^s\frac{\partial^3 u_0}{\partial x^3}+\left(B_{12}^s+2B_{66}^s\right)\frac{\partial^3 u_0}{\partial x\,\partial y^2} \tag{48}$$

$$+B_{22}^{s}\frac{\partial^3 v_0}{\partial y^3}+\left(B_{12}^{s}+2B_{66}^{s}\right)\frac{\partial^3 v_0}{\partial x^2\partial y}-D_{11}^{s}\frac{\partial^4 w_b}{\partial x^4}-2\left(D_{12}^{s}+2D_{66}^{s}\right)\frac{\partial^4 w_b}{\partial x^2\partial y^2}$$
$$-D_{22}^{s}\frac{\partial^4 w_b}{\partial y^4}-H_{11}^{s}\frac{\partial^4 w_s}{\partial x^4}-2\left(H_{12}^{s}+2H_{66}^{s}\right)\frac{\partial^4 w_s}{\partial x^2\partial y^2}-H_{22}^{s}\frac{\partial^4 w_s}{\partial y^4}+A_{44}^{s}\nabla^2 w_s\Bigg]$$
$$+\left(1-\mu_1^2\nabla^2\right)\left(1-\mu_0^2\nabla^2\right)\Bigg[-I_0\left(\ddot{w}_b+\ddot{w}_s\right)-J_1\left(\frac{\partial\ddot{u}_0}{\partial x}+\frac{\partial\ddot{v}_0}{\partial y}\right)+J_2\nabla^2\left(\ddot{w}_b\right) \quad (48)$$
$$+K_2\nabla^2\left(\ddot{w}_s\right)-N^T\nabla^2\left(w_b+w_s\right)-\left(\frac{k_1k_u}{k_1+k_u}\right)\left(w_b+w_s\right)$$
$$+\left(\frac{k_1k_u}{k_1+k_u}\right)\nabla^2\left(w_b+w_s\right)\Bigg]=0$$

They are the equations of wave motion deduced based on refined-higher order shear deformation plate theory and the bi-Helmholtz nonlocal strain gradient theory (B-H NSGT).

4. Solution method

In this section, an exact solution will be presented to solve the equatuons of wave motion for study the wave propagation beahvior of porous FG nanoplates. Here we assume the wave length is relative short and the wave cannot reach the boundary of the nanoplates. That is to say, the boundary conditions will not be considered here. Thus, the solutions with satisfying the displacement fields of the waves propagating in the *x*-*y* plane can be assumed to be the following form

$$\begin{Bmatrix} u_0 \\ v_0 \\ w_b \\ w_s \end{Bmatrix}=\begin{Bmatrix} A_1\exp\left[i\left(k_x x+k_y y-\omega t\right)\right] \\ A_2\exp\left[i\left(k_x x+k_y y-\omega t\right)\right] \\ A_3\exp\left[i\left(k_x x+k_y y-\omega t\right)\right] \\ A_4\exp\left[i\left(k_x x+k_y y-\omega t\right)\right] \end{Bmatrix} \quad (49)$$

in which $i=\sqrt{-1}$; A_1, A_2, A_3, and A_4 are the wave amplitudes; k_x and k_y are the wave numbers of wave propagation along the *x*- and *y*- directions respectively; and ω is the wave frequency. Substituting Eq. (49) into Eqs. (45)-(48), we obtain the governing equations in terms of matrix formula as

$$\mathbf{Ku}=\omega^2\mathbf{Mu} \quad (50)$$

where **K**, **M**, and **u** are the stiffness matrix, mass matrices, and the unknown amplitude vector, respectively. Once the wave frequency is calculated, the phase velocity can be defined as

$$c=\frac{\omega}{k} \quad (51)$$

5. Results and discussion

In this section, the FGM is made of Si_3N_4 and SUS304 with porosities. Using bi-Helmholtz nonlocal strain gradient theory (B-H NSGT) as well as refined-higher order shear deformation plate theory (R-HSDT), numerical results are presented for size-dependent wave propagation of FG nanoplates resting on a gradient hybrid foundation in the thermal environment.

A parametric investigation will be carried out to demonstrate the effects of small-scale parameters (lower and higher order nonlocal parameters and material characteristic parameter), distribution thermal loads (uniform / linear / non-linear / exponential / sinusoidal temperature rise), elastic foundation (gradient hybrid foundation), material distribution index (volume fraction index) on the wave propagation of the perfect and imperfect FG nanoplates. For this purpose, the following dimensionless parameters are used.

$$\tilde{\omega}=\omega a^2\sqrt{\rho_c h/D_c},$$
$$\bar{\omega}=\omega\frac{a^2}{h}\sqrt{\rho_m\left(1-\nu_m^2\right)/E_m}$$
$$\mathrm{K}_l=\frac{k_l a^4}{D_{11}},\mathrm{K}_u=\frac{k_u a^4}{D_{11}},\mathrm{K}_s=\frac{k_s a^2}{D_{11}}$$
$$D_{11}=\left(E_c h^3\right)\Big/\left(12\left(1-\nu_c^2\right)\right)$$

A comparison investigation between the proposed formulations and the open literature is carried out for free vibration of simply supported square FG plate under the influence of thermal load. These results are listed in Table 1. For this purpose, the materials are considered to be temperature dependent, the geometry data are assumed as $a = b = 0.2$ m, $h = 0.025$ m. The dimensionless circular frequency is calculated with the increment of volume fraction index (p) and the temperature of the top surface of the FG plate (T_c). The results obtained using the R-HSDT are compared with those reported by Fazzolari (2016) and Huang and Shen (2004), and an excellent agreement can be observed for the results between the proposed formulations and the open literature.

Table 2 lists the nonlocal dimensionless frequency of imperfect FG plate with porosities (ξ) effect using the present formulation (it is interesting to know that the nonlocal equations are obtained by setting $\mu_1 = l = 0$ in constitutive equations of B-H NSGT). These results are compared with those based on the nonlocal models with CPT, FPT, TPT, SPT and EPT. As can be observed from Table 2, the results of B-H NSGT are in excellent agreement with those reported by Mechab *et al*. (2016).

Hereinafter, the geometry of the FG nanoplates is fixed at $h = 2$ nm, $a = b = 10$ nm (Panyatong *et al*. 2016).

Wave propagation curves of perfect and imperfect FG nanoplate on the basis of different theories are plotted in Fig. 2. The wave numbers (k) change from 0.01 to 100 (1/nm). Here the classical elasticity theory (CET): $\mu_0 = 0$, $\mu_1 = 0$, $l = 0$, nonlocal elasticity theory (NET): $\mu_0 = 1.0$, $\mu_1 = 0$, $l = 0$ nm, strain gradient theory (SGT): $\mu_0 = 0$, $\mu_1 = 0$, $l = 0.2$ nm, and nonlocal strain gradient theory (NSGT): $\mu_0 = 1.0$, $\mu_1 = 0$, $l = 0.2$ nm are taken into consideration. The similar values of small-scale parameters for NET, SGT, and NSGT were used by Li *et al*. (2015) for the wave propagation study of FG nanobeams. Moreover, two groups of data are

Table 1 Dimensionless circular frequency $\bar{\omega}$ parameter for SUS304-Si_3N_4 square plates in thermal environments

p	Method	T_m = 300, T_c = 300	T_m = 300, T_c = 500	T_m = 300, T_c = 600	Error (%)[†]
0	(Huang and Shen 2004)	12.495	12.397	11.984	-
	(Fazzolari 2016)	12.258	12.067	11.667	2.40
	Present	12.3134	12.0607	11.5439	2.61
0.5	(Huang and Shen 2004)	8.675	8.615	8.269	-
	(Fazzolari 2016)	8.505	8.354	8.031	2.62
	Present	8.5340	8.3659	8.0247	2.49
1	(Huang and Shen 2004)	7.555	7.474	7.171	-
	(Fazzolari 2016)	7.473	7.331	7.022	1.69
	Present	7.5020	7.3554	7.0588	1.28
2	(Huang and Shen 2004)	6.777	6.693	6.398	-
	(Fazzolari 2016)	6.716	6.579	6.275	1.51
	Present	6.7514	6.6176	6.3478	0.76
Inf	(Huang and Shen 2004)	5.405	5.311	4.971	-
	(Fazzolari 2016)	5.411	5.270	4.917	0.58
	Present	5.4348	5.3188	5.0288	0.62

Table 2 Dimensionless circular frequency parameter $\tilde{\omega}$ for imperfect and perfect FG nanoplate (a/h = 10, p = 3.5, $(e_0a)^2$ = 1)

ξ	(Mechab *et al*. 2016)	(Mechab *et al*. 2016)	(Mechab *et al*. 2016)	(Mechab *et al*. 2016)	(Mechab *et al*. 2016)	Present
0	11.9045	11.6112	11.5690	11.5671	11.5741	11.6586
0.2	9.56084	9.38471	9.34623	9.34424	9.3508	9.4248

considered for bi-Helmholtz nonlocal strain gradient theory (B-H NSGT) model, that is, B-H NSGT (1): μ_0 = 1.0, μ_1 = 0.5, l = 0.2 nm, and B-H NSGT (2): μ_0 = 1.0, μ_1 = 1.5, l = 0.2 nm. As can be seen in Fig. 2, generally, the phase velocity curves of CET, NET, SGT, NSGT and B-H NSGT are approximately identical when the wave number is about lesser than 1 (1/nm). It shows that, in small wave numbers [k < 1 (1/nm)], the performing calculations by all size-dependent continuum theories lead to almost similar results. This means that wave behaviors of nanostructures (such like nanoplates) are not dependent on their properties in the low wave numbers. Though, in large wave numbers [k > 1 (1/nm)], modified size-dependent continuum theories offer varying graphical trends of phase velocity. As expected, the SGT presents higher values of phase velocity than CET due to the increment in stiffness of nanoplate with considering material characteristic parameter. In the opposite, the NET (which accounts for the interaction between nanoplate atoms on the support of softening-stiffness mechanism) leads to lower phase velocity than CET. These are due to the fact that, with increment in wave number, the dependence of phase velocity to material properties and size effects is increased. Moreover, we can see different trends of phase velocity curves for distinct higher order nonlocal parameters in B-H NSGT (1) and B-H NSGT (2). It is found that, for both perfect and imperfect FG nanoplates, the low value of higher order nonlocal parameter leads to higher phase velocity than the high value of the higher order nonlocal parameter. Besides, with considering porosity volume fraction, the FG nanoplate becomes softer, and as an evident result of that, the phase velocities are decreased. It is important to note that, in comparison with the size effects of small-scale parameters, the influence of porosities can be ignored.

With considering thermal environments, the phase velocities of pure metal/-ceramic, as well as perfect and imperfect FG nanoplates under the influence of different distributions of temperature rise, are calculated as a function of wave number. These results are shown in Figs. 3(a)-(d). As a conclusion, both of temperature-dependent isotropic and graded nanoplates without thermal effect have larger phase velocities than the counterparts including thermal effect. This effect in lower values of wave number is evident, while a non-significant influence is observed on the phase velocities for large wave numbers. As observed, the sinusoidal model performs higher phase velocities than other temperature rise distribution, followed by nonlinear, linear, exponential, and uniform, respectively. It is clear that the effect of temperature is more significant in fully ceramic (p = 0) in comparison with the pure metal (p = ∞). Moreover, in the high values of wave numbers, volume fraction index p and porosity volume fraction ξ play a dominant role in the results and lead to sharp decrement and increment on phase velocities, respectively. Furthermore, an increment in porosity volume fraction is proportional to the decrement in the peak value of phase velocity. The increment in material gradient index yields the decrease in the volume fraction of ceramic phase that leads to the

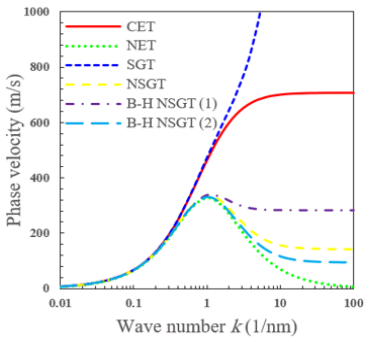

(a) Perfect FG nanoplate

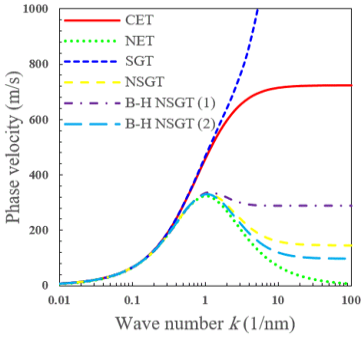

(b) Imperfect FG nanoplate

Fig. 2 Phase velocity response versus the wave number for room temperature ($T_m = T_c = 300$ K) based on classical elasticity theory (CET), nonlocal elasticity theory (NET), strain gradient theory (SGT), nonlocal strain gradient theory (NSGT), bi-Helmholtz nonlocal strain gradient theory (B-H NSGT) (1), and B-H NSGT (2) for: (a**)** perfect FG nanoplate ($p = 1$, $\xi = 0$); (b**)** imperfect FG nanoplate ($p = 1$, $\xi = 0.2$)

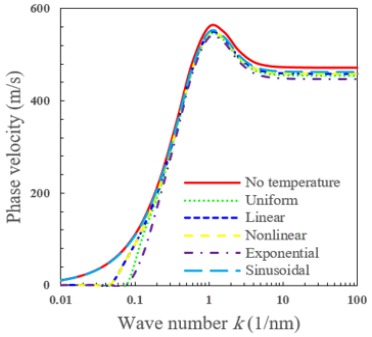

(a) Fully ceramic nanoplate

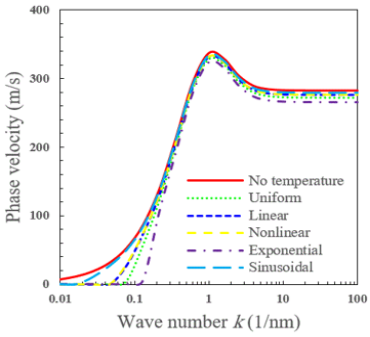

(b) Perfect FG nanoplate

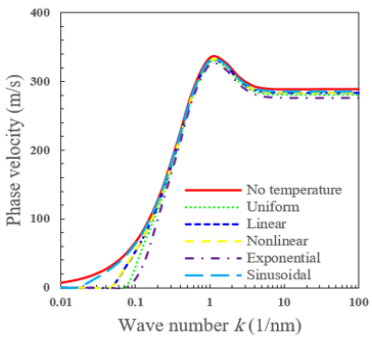

(c) Imperfect FG nanoplate

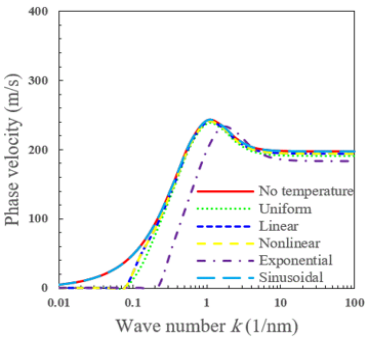

(d) Fully metal nanoplate

Fig. 3 Influence of temperature rise distribution against wave number in $T_c = 500$ K for: (a**)** fully ceramic nanoplate ($p = 0$, $\xi = 0$); (b) perfect FG nanoplate ($p = 1$, $\xi = 0$); (c**)** imperfect FG nanoplate ($p = 1$, $\xi = 0.2$); and (d**)** fully metal nanoplate ($p = \infty$, $\xi = 0$)

decrement in bending rigidity and phase velocity of the FG nanoplate.

To show the effect of foundation on the phase velocities, a variation of phase velocities of embedded perfect and imperfect FG nanoplate for different values of spring constants and shear layer parameter is plotted in Fig. 4. For the sake of simplicity, the stiffness of lower and upper springs of gradient hybrid foundation are the same. Generally, including a foundation grows the phase velocity of the FG nanoplate. This increment is related to the hardness effect of each foundation. So, a nanoplate with foundation is stiffer than the counterpart without foundation. As can be seen from Fig. 4, the low and high values of springs and shear layer parameter have rising effects on the phase velocities of imperfect and perfect FG nanoplates. This efficiency is easily visible in low values of wave number. Moreover, due to the figure, it is concluded that, in the case of low wave numbers, the wave behavior of imperfect FG nanoplates depends significantly on the values of the foundation parameters, especially at the range of soft and moderate stiffness for springs and shear layer. However, the change trend of phase velocity for both soft and hard foundations remains relatively constant.

(a) Perfect FG nanoplate (b) Imperfect FG nanoplate

Fig. 4 Influence of gradient hybrid foundation parameters against wave number in T_c = 300 K for: (a**)** perfect FG nanoplate (p = 1, ξ = 0); (b**)** imperfect FG nanoplate (p = 1, ξ = 0.2)

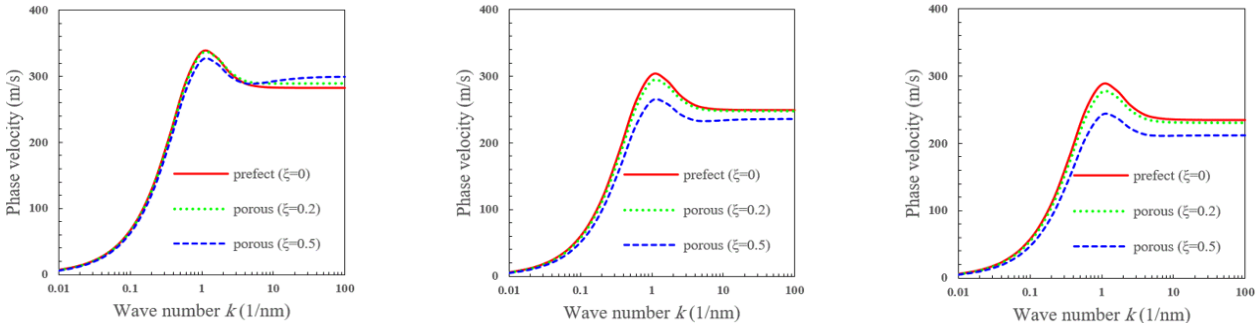

(a) p = 1 (b) p = 2 (c) p = 3

Fig. 5 Mutation of volume fraction index (p) versus wave number in T_c = 300 K for various values of porosity volume fraction (ξ)

(a) Lower order nonlocal parameter (b) Higher order nonlocal parameter

Fig. 6 Influence of material characteristic parameter on the phase velocity response of the imperfect FG nanoplate exposed to the nonlinear thermal loading (T_c = 500 K) versus: (a**)** lower order nonlocal parameter; and (b**)** higher order nonlocal parameter, (k = 2(1/nm) p = 1, ξ = 0.2, K_l = 10, K_u = 10, K_s = 5)

Fig. 5 depicts the variation of phase velocity for imperfect and perfect FG nanoplates with increasing volume fraction index and porosity volume fraction. It is easily understood that with the enhancement in the value of volume fraction index phase velocities will decrease. This is due to the fact that the higher volume fraction index means the nanoplate has more metal contents and stiffness will reduce, and hence phase velocities will decrease. It is noteworthy that when the wave number is very small [k < 0.1 (1/nm)], the effect of porosity is unimportant but its effect keeps on increasing as the wave number increases.

In the case of a constant wave number [k = 2 (1/nm)] and the nonlinear thermal loading, Fig. 6 shows the influence of material characteristic parameter on the phase velocity response of the imperfect FG nanoplate. Under the circumstances, the impact factors of lower and higher order nonlocal parameters are more significant than those in the absence and presence of material parameter, respectively. Despite that the lower order nonlocal parameter is an independent parameter, the higher order nonlocal parameter has no significant effect on the phase velocity in absence of the material characteristic parameter.

6. Conclusions

A high-order nonlocal strain gradient model was developed to studying the wave propagation of functionally graded (FG) nanoplates. The FG nanoplates considered here is porous and supported by a gradient hybrid foundation within thermal environment. On the basis of the refined-higher order shear deformation plate theory (R-HSDT) in conjunction with the bi-Helmholtz nonlocal strain gradient theory (B-H NSGT), the equations of wave motion are derived by using Hamilton's principle. Then, the influences of various parameters on the wave propagation behaviors of porous FG nanoplates are investigated in detail. On the basis of the parametric investigations, the following conclusions can be notable.

- With the increment in nonlocal parameters (material characteristic parameter), the FG nanoplate becomes stiffer (softer).
- When omitting the material characteristic parameter from fundamental equations, the lower (higher) order nonlocal parameter has (does not have) important effect on the phase velocity results.
- The increment of temperature, volume fraction index and porosity volume fraction (spring constants and shear layer parameter) will lead to the lower (higher) phase velocities.
- When the FG nanoplate is surrounded by a hard foundation, as a paradox conclusion, the phase velocity in low wave numbers increases with the increase of the porosity volume fraction.
- The influence of environmental loading and foundation components (small-scale parameters, volume fraction index and porosity volume fraction) on the phase velocities increase with the decrement (increment) of the wave numbers, respectively.
- The sinusoidal scenario for determining temperature rise distribution performs higher phase velocities than other temperature rise distributions, followed by nonlinear, linear, exponential, and uniform, respectively.

References

Askes, H. and Aifantis, E.C. (2009), "Gradient elasticity and flexural wave dispersion in carbon nanotubes", *Phys. Rev. B*, **80**(19), 195412.

Azadi, V., Azadi, M., Fazelzadeh, S.A. and Azadi, E. (2014), "Active control of an fgm beam under follower force with piezoelectric sensors/actuators", *Int. J. Struct. Stabil. Dyn.*, **14**(2), 1350063.

Barati, M.R. (2017a), "On wave propagation in nanoporous materials", *Int. J. Eng. Sci.*, **116**, 1-11.

Barati, M.R. (2017b), "Vibration analysis of FG nanoplates with nanovoids on viscoelastic substrate under hygro-thermo-mechanical loading using nonlocal strain gradient theory", *Struct. Eng. Mech., Int. J.*, **64**(6), 683-693.

Barati, M.R. and Zenkour, A. (2017), "A general bi-Helmholtz nonlocal strain-gradient elasticity for wave propagation in nanoporous graded double-nanobeam systems on elastic substrate", *Compos. Struct.*, **168**, 885-892.

Bellifa, H., Bakora, A., Tounsi, A., Bousahla, A.A. and Mahmoud, S. (2017), "An efficient and simple four variable refined plate theory for buckling analysis of functionally graded plates", *Steel Compos. Struct., Int. J.*, **25**(3), 257-270.

Bhattacharyya, M., Kapuria, S. and Kumar, A. (2007), "On the stress to strain transfer ratio and elastic deflection behavior for Al/SiC functionally graded material", *Mech. Adv. Mater. Struct.*, **14**(4), 295-302.

Ebrahimi, F. and Dabbagh, A. (2018), "Wave dispersion characteristics of nonlocal strain gradient double-layered graphene sheets in hygro-thermal environments", *Struct. Eng. Mech., Int. J.*, **65**(6), 645-656.

Elmossouess, B., Kebdani, S., Bouiadjra, M.B. and Tounsi, A. (2017), "A novel and simple HSDT for thermal buckling response of functionally graded sandwich plates". *Struct. Eng. Mech., Int. J.*, **62**(4), 401-415.

Eringen, A.C. (1983), "On differential equations of nonlocal elasticity and solutions of screw dislocation and surface waves", *J. Appl. Phys.*, **54**(9), 4703-4710.

Farokhi, H. and Ghayesh, M.H. (2015), "Thermo-mechanical dynamics of perfect and imperfect Timoshenko microbeams", *Int. J. Eng. Sci.*, **91**, 12-33.

Farokhi, H., Ghayesh, M.H. and Amabili, M. (2013), "Nonlinear dynamics of a geometrically imperfect microbeam based on the modified couple stress theory", *Int. J. Eng. Sci.*, **68**, 11-23.

Fazzolari, F.A. (2016), "Modal characteristics of P-and S-FGM plates with temperature-dependent materials in thermal environment", *J. Thermal Stresses*, **39**(7), 854-873.

Ghayesh, M.H. (2018a), "Dynamics of functionally graded viscoelastic microbeams", *Int. J. Eng. Sci.*, **124**, 115-131.

Ghayesh, M.H. (2018b), "Functionally graded microbeams: simultaneous presence of imperfection and viscoelasticity", *Int. J. Mech. Sci.*, **140**, 339-350.

Ghayesh, M.H. (2018c), "Mechanics of tapered AFG shear-deformable microbeams", *Microsyste. Technol.*, **24**(4), 1743-1754.

Ghayesh, M.H. (2018d), "Nonlinear vibration analysis of axially functionally graded shear-deformable tapered beams", *Appl. Math. Model.*, **59**, 583-596.

Ghayesh, M.H., Amabili, M. and Farokhi, H. (2013a), "Nonlinear forced vibrations of a microbeam based on the strain gradient elasticity theory", *Int. J. Eng. Sci.*, **63**, 52-60.

Ghayesh, M.H., Amabili, M. and Farokhi, H. (2013b), "Three-dimensional nonlinear size-dependent behaviour of Timoshenko microbeams", *Int. J. Eng. Sci.*, **71**, 1-14.

Ghayesh, M.H., Farokhi, H. and Amabili, M. (2013c), "Nonlinear behaviour of electrically actuated MEMS resonators", *Int. J. Eng. Sci.*, **71**, 137-155.

Ghayesh, M.H., Farokhi, H. and Amabili, M. (2013d), "Nonlinear dynamics of a microscale beam based on the modified couple stress theory", *Compos. Part B: Eng.*, **50**, 318-324.

Ghayesh, M.H., Farokhi, H. and Amabili, M. (2014), "In-plane and out-of-plane motion characteristics of microbeams with modal interactions", *Compos. Part B: Eng.*, **60**, 423-439.

Ghayesh, M.H., Farokhi, H. and Gholipour, A. (2017), "Oscillations of functionally graded microbeams", *Int. J. Eng. Sci.*, **110**, 35-53.

Gholipour, A., Farokhi, H. and Ghayesh, M.H. (2015), "In-plane and out-of-plane nonlinear size-dependent dynamics of microplates", *Nonlinear Dyn.*, **79**(3), 1771-1785.

Gupta, A. and Talha, M. (2017), "Influence of porosity on the flexural and free vibration responses of functionally graded plates in thermal environment", *Int. J. Struct. Stabil. Dyn.*, 1850013.

Hachemi, H., Kaci, A., Houari, M.S.A., Bourada, M., Tounsi, A. and Mahmoud, S. (2017), "A new simple three-unknown shear deformation theory for bending analysis of FG plates resting on

elastic foundations", *Steel Compos. Struct., Int. J.*, **25**(6), 717-726.

Huang, X.-L. and Shen, H.-S. (2004), "Nonlinear vibration and dynamic response of functionally graded plates in thermal environments", *Int. J. Solids Struct.*, **41**(9), 2403-2427.

Kapuria, S., Bhattacharyya, M. and Kumar, A. (2008), "Bending and free vibration response of layered functionally graded beams: a theoretical model and its experimental validation", *Compos. Struct.*, **82**(3), 390-402.

Karami, B. and Janghorban, M. (2016), "Effect of magnetic field on the wave propagation in nanoplates based on strain gradient theory with one parameter and two-variable refined plate theory", *Modern Phys. Lett. B*, **30**(36), 1650421.

Karami, B., Janghorban, M. and Tounsi, A. (2017), "Effects of triaxial magnetic field on the anisotropic nanoplates", *Steel Compos. Struct., Int. J.*, **25**(3), 361-374.

Karami, B., Janghorban, M. and Li, L. (2018a), "On guided wave propagation in fully clamped porous functionally graded nanoplates", *Acta Astronautica*, **143**, 380-390.

Karami, B., Janghorban, M., Shahsavari, D. and Tounsi, A. (2018b), "A size-dependent quasi-3D model for wave dispersion analysis of FG nanoplates", *Steel Compos. Struct., Int. J.*, **28**(1), 99-110.

Karami, B., Janghorban, M. and Tounsi, A. (2018c), "Nonlocal strain gradient 3D elasticity theory for anisotropic spherical nanoparticles", *Steel Compos. Struct., Int. J.*, **27**(2), 201-216.

Karami, B., Janghorban, M. and Tounsi, A. (2018d), "Variational approach for wave dispersion in anisotropic doubly-curved nanoshells based on a new nonlocal strain gradient higher order shell theory", *Thin-Wall. Struct.*, **129**, 251-264.

Karami, B., Shahsavari, D. and Janghorban, M. (2018e), "Wave propagation analysis in functionally graded (FG) nanoplates under in-plane magnetic field based on nonlocal strain gradient theory and four variable refined plate theory", *Mech. Adv. Mater. Struct.*, **25**(12), 1047-1057.

Karami, B., Shahsavari, D., Janghorban, M. and Li, L. (2018f), "Wave dispersion of mounted graphene with initial stress", *Thin-Wall. Struct.*, **122**, 102-111.

Karami, B., Shahsavari, D., Karami, M. and Li, L. (2018g), "Hygrothermal wave characteristic of nanobeam-type inhomogeneous materials with porosity under magnetic field", *Proceedings of the Institution of Mechanical Engineers, Part C: J. Mech. Eng. Sci.*, 0954406218781680.

Karami, B., Shahsavari, D. and Li, L. (2018h), "Hygrothermal wave propagation in viscoelastic graphene under in-plane magnetic field based on nonlocal strain gradient theory", *Physica E: Low-dimensional Syst. Nanostruct.*, **97**, 317-327.

Karami, B., Shahsavari, D. and Li, L. (2018i), "Temperature-dependent flexural wave propagation in nanoplate-type porous heterogenous material subjected to in-plane magnetic field", *J. Thermal Stresses*, **41**(4), 483-499.

Karami, B., Shahsavari, D., Li, L., Karami, M. and Janghorban, M. (2018j), "Thermal buckling of embedded sandwich piezoelectric nanoplates with functionally graded core by a nonlocal second-order shear deformation theory", *Proceedings of the Institution of Mechanical Engineers, Part C: J. Mech. Eng. Sci.*, 0954406218756451.

Klouche, F., Darcherif, L., Sekkal, M., Tounsi, A. and Mahmoud, S. (2017), "An original single variable shear deformation theory for buckling analysis of thick isotropic plates", *Struct. Eng. Mech., Int. J.*, **63**(4), 439-446.

Koutsoumaris, C.C., Vogiatzis, G., Theodorou, D., Tsamasphyros, G., Simos, T.E., Kalogiratou, Z. and Monovasilis, T. (2015), "Application of bi-Helmholtz nonlocal elasticity and molecular simulations to the dynamical response of carbon nanotubes", *AIP Conference Proceedings*, AIP Publishing, 190011.

Lam, D.C.C., Yang, F., Chong, A., Wang, J. and Tong, P. (2003), "Experiments and theory in strain gradient elasticity", *J. Mech. Phys. Solids*, **51**(8), 1477-1508.

Lazar, M., Maugin, G.A. and Aifantis, E.C. (2006), "On a theory of nonlocal elasticity of bi-Helmholtz type and some applications", *Int. J. Solids Struct.*, **43**(6), 1404-1421.

Li, L. and Hu, Y. (2016a), "Nonlinear bending and free vibration analyses of nonlocal strain gradient beams made of functionally graded material", *Int. J. Eng. Sci.*, **107**, 77-97.

Li, L. and Hu, Y. (2016b), "Wave propagation in fluid-conveying viscoelastic carbon nanotubes based on nonlocal strain gradient theory", *Computat. Mater. Sci.*, **112**, 282-288.

Li, J.F., Takagi, K., Ono, M., Pan, W., Watanabe, R., Almajid, A. and Taya, M. (2003), "Fabrication and evaluation of porous piezoelectric ceramics and porosity–graded piezoelectric actuators", *J. Am. Ceramic Soc.*, **86**(7), 1094-1098.

Li, Q., Iu, V. and Kou, K. (2009), "Three-dimensional vibration analysis of functionally graded material plates in thermal environment", *J. Sound Vib.*, **324**(3), 733-750.

Li, L., Hu, Y. and Ling, L. (2015), "Flexural wave propagation in small-scaled functionally graded beams via a nonlocal strain gradient theory", *Compos. Struct.*, **133**, 1079-1092.

Li, L., Hu, Y. and Ling, L. (2016), "Wave propagation in viscoelastic single-walled carbon nanotubes with surface effect under magnetic field based on nonlocal strain gradient theory", *Physica E: Low-dimensional Syst. Nanostruct.*, **75**, 118-124.

Lim, C., Zhang, G. and Reddy, J. (2015), "A higher-order nonlocal elasticity and strain gradient theory and its applications in wave propagation", *J. Mech. Phys. Solids*, **78**, 298-313.

Lin, Q.-Y., Jing, G., Zhou, Y.-B., Wang, Y.-F., Meng, J., Bie, Y.-Q., Yu, D.-P. and Liao, Z.-M. (2013), "Stretch-induced stiffness enhancement of graphene grown by chemical vapor deposition", *ACS Nano*, **7**(2), 1171-1177.

Mechab, I., Atmane, H.A., Tounsi, A. and Belhadj, H.A. (2010), "A two variable refined plate theory for the bending analysis of functionally graded plates", *Acta Mech. Sinica*, **26**(6), 941-949.

Mechab, I., Mechab, B., Benaissa, S., Serier, B. and Bouiadjra, B.B. (2016), "Free vibration analysis of FGM nanoplate with porosities resting on Winkler Pasternak elastic foundations based on two-variable refined plate theories", *J. Brazil. Soc. Mech. Sci. Eng.*, **8**(38), 2193-2211.

Meftah, A., Bakora, A., Zaoui, F.Z., Tounsi, A. and Bedia, E.a.A. (2017), "A non-polynomial four variable refined plate theory for free vibration of functionally graded thick rectangular plates on elastic foundation", *Steel Compos. Struct., Int. J.*, **23**(3), 317-330.

Merdaci, S., Tounsi, A. and Bakora, A. (2016), "A novel four variable refined plate theory for laminated composite plates", *Steel Compos. Struct., Int. J.*, **22**(4), 713-732.

Nami, M.R. and Janghorban, M. (2014), "Wave propagation in rectangular nanoplates based on strain gradient theory with one gradient parameter with considering initial stress", *Modern Phys. Lett. B*, **28**(03), 1450021.

Narendar, S. and Gopalakrishnan, S. (2012), "Scale effects on buckling analysis of orthotropic nanoplates based on nonlocal two-variable refined plate theory", *Acta Mechanica*, **223**(2), 395-413.

Panyatong, M., Chinnaboon, B. and Chucheepsakul, S. (2016), "Free vibration analysis of FG nanoplates embedded in elastic medium based on second-order shear deformation plate theory and nonlocal elasticity", *Compos. Struct.*, **153**, 428-441.

Praveen, G. and Reddy, J. (1998), "Nonlinear transient thermoelastic analysis of functionally graded ceramic-metal plates", *Int. J. Solids Struct.*, **35**(33), 4457-4476.

Rad, A.B. (2015), "Thermo-elastic analysis of functionally graded circular plates resting on a gradient hybrid foundation", *Appl. Math. Computat.*, **256**, 276-298.

Reddy, J. and Chin, C. (1998), "Thermomechanical analysis of

functionally graded cylinders and plates", *J. Thermal Stresses*, **21**(6), 593-626.
Sarangan, S. and Singh, B. (2016), "Higher-order closed-form solution for the analysis of laminated composite and sandwich plates based on new shear deformation theories", *Compos. Struct.*, **138**, 391-403.
Sehoul, M., Benguediab, M., Bakora, A. and Tounsi, A. (2017), "Free vibrations of laminated composite plates using a novel four variable refined plate theory", *Steel Compos. Struct., Int. J.*, **24**(5), 603-613.
Sekkal, M., Fahsi, B., Tounsi, A. and Mahmoud, S. (2017), "A novel and simple higher order shear deformation theory for stability and vibration of functionally graded sandwich plate", *Steel Compos. Struct., Int. J.*, **25**(4), 389-401.
Shahsavari, D. and Janghorban, M. (2017), "Bending and shearing responses for dynamic analysis of single-layer graphene sheets under moving load", *J. Brazil. Soc. Mech. Sci. Eng.*, **39**(10), 3849-3861.
Shahsavari, D., Karami, B., Janghorban, M. and Li, L. (2017), "Dynamic characteristics of viscoelastic nanoplates under moving load embedded within visco-Pasternak substrate and hygrothermal environment", *Mater. Res. Express*, **4**(8), 085013.
Shahsavari, D., Karami, B. and Mansouri, S. (2018a), "Shear buckling of single layer graphene sheets in hygrothermal environment resting on elastic foundation based on different nonlocal strain gradient theories", *Eur. J. Mech.-A/Solids*, **67**, 200-214.
Shahsavari, D., Shahsavari, M., Li, L. and Karami, B. (2018b), "A novel quasi-3D hyperbolic theory for free vibration of FG plates with porosities resting on Winkler/Pasternak/Kerr foundation", *Aerosp. Sci. Technol.*, **72**, 134-149.
She, G.-L., Yuan, F.-G., Ren, Y.-R. and Xiao, W.-S. (2017), "On buckling and postbuckling behavior of nanotubes", *Int. J. Eng. Sci.*, **121**, 130-142.
She, G.-L., Ren, Y.-R., Yuan, F.-G. and Xiao, W.-S. (2018), "On vibrations of porous nanotubes", *Int. J. Eng. Sci.*, **125**, 23-35.
Shimpi, R.P. (2002), "Refined plate theory and its variants", *AIAA Journal*, **40**(1), 137-146.
Shimpi, R. and Patel, H. (2006a), "Free vibrations of plate using two variable refined plate theory", *J. Sound Vib.*, **296**(4), 979-999.
Shimpi, R. and Patel, H. (2006b), "A two variable refined plate theory for orthotropic plate analysis", *Int. J. Solids Struct.*, **43**(22-23), 6783-6799.
Thai, H.-T. and Kim, S.-E. (2012), "Analytical solution of a two variable refined plate theory for bending analysis of orthotropic Levy-type plates", *Int. J. Mech. Sci.*, **54**(1), 269-276.
Touloukian, Y.S. and Ho, C. (1970), "Thermal expansion. Nonmetallic solids", *Thermophysical properties of matter-The TPRC Data Series, New York: IFI/Plenum, 1970-, edited by Touloukian, YS| e (series ed.); Ho, CY| e (series tech. ed.).*
Wattanasakulpong, N. and Ungbhakorn, V. (2014), "Linear and nonlinear vibration analysis of elastically restrained ends FGM beams with porosities", *Aerosp. Sci. Technol.*, **32**(1), 111-120.
Yahia, S.A., Atmane, H.A., Houari, M.S.A. and Tounsi, A. (2015), "Wave propagation in functionally graded plates with porosities using various higher-order shear deformation plate theories", *Struct. Eng. Mech., Int. J.*, **53**(6), 1143-1165.
Zhu, X. and Li, L. (2017), "Closed form solution for a nonlocal strain gradient rod in tension", *Int. J. Eng. Sci.*, **119**, 16-28.
Zhu, J., Lai, Z., Yin, Z., Jeon, J. and Lee, S. (2001), "Fabrication of ZrO 2–NiCr functionally graded material by powder metallurgy", *Mater. Chem. Phys.*, **68**(1), 130-135.
Zidi, M., Houari, M.S.A., Tounsi, A., Bessaim, A. and Mahmoud, S. (2017), "A novel simple two-unknown hyperbolic shear deformation theory for functionally graded beams", *Struct. Eng. Mech., Int. J.*, **64**(2), 145-153.

CC